Applied Catalysis B: Environmental 258 (2019) 117971

Contents lists available at ScienceDirect

Applied Catalysis B: Environmental

journal homepage: www.elsevier.com/locate/apcatb

Differences in bifunctionality of ZnO and ZrO_2 in $Cu/ZnO/ZrO_2/Al_2O_3$ catalysts in hydrogenation of carbon oxides for methanol synthesis

Imran Abbas[a,b], Honggon Kim[a], Chae-Ho Shin[c], Sungho Yoon[d], Kwang-Deog Jung[a,b,*]

[a] Clean Energy Research Center, Korea Institute of Science and Technology, Hwarangno 14-gil 5, Seongbuk-gu, Seoul 136-791, Republic of Korea
[b] Clean Energy and Chemical Engineering, University of Science and Technology, 217 Gajeong-ro Yuseong-gu, Daejeon, Republic of Korea
[c] Department of Chemical Engineering, Chungbuk Natinal University,Chungdae-ro 1, Seowon-Gu, Cheongju, Chungbuk 28644, Republic of Korea
[d] Department of Applied Chemistry, Kookmin University, 77 Jeongneung-ro, Sungbuk-gu, Seoul 02707, Republic of Korea

ARTICLE INFO

Keywords:
Methanol synthesis
CO_2 hydrogenation
$Cu/ZnO/ZrO_2/Al_2O_3$
Hydrogen spillover

ABSTRACT

This work investigates the promotional roles of ZrO_2 and ZnO for methanol synthesis on five $Cu_6Zn_{3.0-x}Zr_xAl_1$ (x = 0.0, 0.5, 1.5, 2.5, 3.0) catalysts in the various CO_2 feed composition. TOF decreased with an increase in x of $Cu_6Zn_{3.0-x}Zr_xAl_1$ catalysts in the 5% CO_2 feed, while TOF is maximized over $Cu_6Zn_{1.5}Zr_{1.5}Al_1$ in the 100% CO_2 feed. Both the effects of Zn (reverse spillover) and Zr (additional reaction sites) in the vicinity of Cu promote the CO_2 hydrogenation, maximizing the catalytic activity of $Cu_6Zn_{1.5}Zr_{1.5}Al_1$ in the 100% CO_2 feed. The migration of hydrogen on ZrO_2 can be limited in little surface hydroxyls in 5% CO_2 feed, which can be a reason for the negative role of ZrO_2 in the 5% CO feed. The promotional effect of ZrO_2 on Cu/ZnO is important only for high CO_2 feed more than 50% CO_2.

1. Introduction

Methanol is a key chemical intermediate to synthesize formaldehyde, Methyl tert-butyl ether (MTBE), tert-Amyl methyl ether (TAME), acetic acid and dimethyl ether consuming about 80 million tons/year in 2018 [1]. Moreover, the demand for methanol as a raw material for fuel additives and MTO process has increased [2]. On the other hand, hydrogen has been considered as a promising sustainable alternative of fossil fuels associated with the transportation [3]. Methanol has also become a plausible candidate for the storage of H_2 [4–6], because it is in liquid state at room temperature and has a freezing point around -98 °C [7]. Additionally, methanol can be used for the reuse of CO_2 in term of methanol economy for a carbon cycle [5,8–10], because CO_2 is a primary source for methanol synthesis. Even in CO_2 hydrogenation process for methanol economy using CO_2 as media as hydrogen carrier, CO/CO_2 hydrogenation should also be considered in the process, because the syngas from the exit of the reactor should be recycled to the reactor. Therefore, even though CO_2 hydrogenation to methanol is important for the purpose of hydrogen storage, CO/CO_2 hydrogenation should also be considered for the practical process development.

Industrially, methanol is produced by hydrogenation of synthesis gas at 200–300 °C and 50–100 at m over $Cu/ZnO/Al_2O_3$ catalysts [11–13]. Methanol synthesis has been studied for over a century, but this reaction is not fully understood mechanismically and there are many aspects being debated to date [14–25].

In the beginning, CO was considered as the carbon source of methanol [26] until isotope labelling experiments showed that CO_2 was mainly hydrogenated to methanol [12,27]. Recently, many researchers have agreed that CO_2 is a primary carbon source for methanol synthesis [28].

It was suggested that Cu^+ is the active site for methanol synthesis [26,29], but intrinsic methanol synthesis was found to be proportional to Cu surface area irrespective of the different kinds of Cu sites [30]. Studies of methanol synthesis over Cu(111), Cu(110) and Cu(100) suggested that the reaction was structure sensitive with the assumption that metallic Cu is an active site only [31–34]. Fujitani et al. deposited Zn on Cu(111) and Cu(110) and proposed synergistic effect between Cu and ZnO [35,36]. However, Chinchen et al. showed that Cu supported on either SiO_2 or MgO is as active as that on ZnO in the feed composition with high H_2 content in the practical methanol synthesis [37], concluding that methanol synthesis is structure insensitive in the feed with high H_2 content on Cu based catalysts. In methanol synthesis, the structure insensitivity on Cu/ZnO was clearly observed on the Cu/ZnO catalysts with Zn content higher than 10% molar concentration on Cu/ZnO [20]. On the other hand, ZnO was reported to help stabilize Cu^+

* Corresponding author at: Clean Energy Research Center, Korea Institute of Science and Technology, Hwarangno 14-gil 5, Seongbuk-gu, Seoul 136-791, Republic of Korea.
E-mail address: jkdcat@kist.re.kr (K.-D. Jung).

https://doi.org/10.1016/j.apcatb.2019.117971
Received 13 December 2018; Received in revised form 14 June 2019; Accepted 16 July 2019
Available online 17 July 2019

[26]. Depending on the oxidation state of surrounding gas, it was suggested that ZnO helped to induce structural changes of Cu particles [38]. Behrens et al. claimed that Cu kinks, terraces and defects decorated with ZnO was the active site for methanol synthesis, suggesting the structure sensitivity [13]. Recently, it was again claimed that surface Zn transformed to ZnO and CuZnO, which was the cause of the synergic effect in methanol synthesis [22]. The H/D exchange and formate spillover between Cu and ZnO has also been discussed [39,40]. Spencer (ICI) proposed the reverse hydrogen spillover from ZnO to Cu to explain synergistic effects in CO_2 hydrogenation in CO2 hydrogenation [41].

Some studies on Cu/MgO and Cu/CeOx claimed that methanol synthesis was strongly structure sensitive, suggesting that the combination of metal and oxide sites in the copper-ceria interface afforded complementary chemical properties that lead to special reaction pathways for the conversion of CO_2 to CH_3OH [42]. It was also claimed that the structure sensitive behaviors were dependent on the basicity and acidity of supports [15]. Cu/MgO with strong basic sites exhibited the highest activity with pure CO only, but it showed the negligible activity in the presence of CO_2. On the other hand, Cu/Al_2O_3 with acidic support exhibited very low activity in all the $CO_2/(CO_2+CO)$ composition. However, the catalytic activity of ZnO added Cu/MgO catalysts increased with increasing CO_2 content in the feed, differently from Cu/MgO. From these observations, the importance of basic metal oxide supports was emphasized for methanol synthesis on Cu based catalysts. Recently, LDH supported CuZnZr system gave the high Cu dispersion and exhibited high activity for CO2 hydrogenation [43]. It was suggested that the high adsorption capability of LDH was the reason for the high methanol productivity in CO_2 hydrogenation. The modulation of basic sites in $Cu/ZnO/Al_2O_3$ also improved the dispersion of Cu and stabilized Cu^{+1} to enhance methanol yields [44], emphasizing the importance of basic sites. Recent work on $Cu/ZnAl_2O_4$ also supported the importance of metal oxide supports [45].

IR analysis and TPD analysis observed Cu-formate, Zn-formate and Zn-methoxy in CO_2/H_2, while Zn-formate and Zn-methoxy only in CO/H_2 [46]. ZnO alone showed formate on ZnO but no methoxy, suggesting that hydrogen spillover to ZnO from Cu was necessary to form Zn-methoxy. Burch et. al also claimed the hydrogen spillover to ZnO in methanol synthesis and spilt hydrogens were trapped on ZnO for the reverse hydrogen spillover [41,47].

Similar to Cu/ZnO, ZrO_2 is classified as amphoteric oxide and it was shown that the structure of ZrO_2 significantly affected methanol synthesis [48]. The hydrogen spillover from Cu to ZrO_2 was observed with H/D exchange reaction and the importance of hydroxyls on the ZrO_2 surface was emphasized for the hydrogen migration, showing that hydrogen migrations to form Zr-methoxy decreased after CO was inserted into metal hydroxyl to form Zr-formate, depleting the surface hydroxyls for the hydrogen migration [49]. Difference of hydrogen spillover rate of Cu/m-ZrO_2 and Cu/t-ZrO_2 reflected the catalytic CO_2 hydrogenation for methanol synthesis: Cu/m-ZrO_2 was 4 times higher than Cu/t-ZrO_2 [50], suggesting the importance of hydroxyls on the metal oxide support. Recent studies on Cu/ZrO_2 reported the structural effect of ZrO_2 in methanol synthesis. It was reported that Cu/t-ZrO_2 was more active than Cu/m-ZrO_2 [49]. Additionally, Cu/a-ZrO_2 (amorphous ZrO_2) was the most active among the three ZrO_2 phases of m-ZrO_2, t-ZrO_2 and a-ZrO_2 [52,53]. The t-ZrO_2 phase can be stabilized by the presence of oxygen vacancies, which can stabilize Cu^{+1} [51]. It was also concluded that the interfacial sites between Cu and ZrO_2 can be specific active sites for methanol synthesis [53]. The addition of WO_3 to $Cu/ZnO/ZrO_2$ induced the formation of ZnO-ZrO_2 resulting in high Cu dispersion [54]. It was proposed that the catalytic activity of $Cu/ZnO/ZrO_2/WO_3$ system was closely related to the Cu metallic surface area, amount of weak basic sites and reducibility of the catalysts.

However, there have been controversy on the hydrogen spillover on nonreducible metal oxides such as SiO_2 and Al_2O_3 without defect sites [55]. Juhwan Im et. al. showed that the hydrogen spillover onto the nonreducible aluminsilicate becomes energetically viable (overall activation energy < 0.98 eV) without involving a series of hemolytic bond dissociation and formation process (> ~5 eV) [56]. Additionally to that, hydrogen spillover from Pt to alumina support clearly showed that hydrogen spillover could be mediated vis three-coordinated surface aluminum adsorption sites [57], exhibiting that the hydrogen spillover via alumina and silica from Pt was not energetically impossible. They mentioned that the conclusion on no hydrogen spillover to nonreducible oxides such as SiO_2 and Al_2O_3 was based on the oversimplified assumption.

Here, we attempted to investigate both structural (stabilization of Cu/Cu^{+1}) and kinetic (hydrogen spillover) effects of ZrO_2 to assist Cu/ZnO catalytic system. For the purpose, we prepared five catalyst with $CuO:ZnO:ZrO_2:Al_2O_3$ molar ratio (a) 6:3:0:1, (b) 6:2.5:0.5:1, (c) 6:1.5:1.5:1, (d) 6:0.5:2.5:1 and (e) 6:0:3:1. Prepared catalysts were named as $Cu_6Zn_{3-x}Zr_xAl_1$ where x = 0.0, 0.5, 1.5, 2.5, and 3.0 for (a), (b), (c), (d) and (e), respectively.

We investigated the kinetic effect of ZrO_2 (amphoteric support) with the prepared catalysts depending on CO_2 contents in CO_2/CO feed gas at a very high GHSV to minimize shift reaction. Structural effects of ZrO_2 to assist Cu/ZnO system were also monitored with temperature programmed reduction, in-situ XRD and TEM analysis and the activity of the prepared catalysts was compared in a wide range of CO and CO_2 composition at the fixed R ratio $((H_2-CO_2)/(CO+CO_2))$ of 2.0. Structure sensitivity of methanol synthesis over $CuO/ZnO/ZrO_2/Al_2O_3$ catalysts on different CO/CO_2 compositions was discussed.

2. Experimental

2.1. Catalyst preparation of CuZnZrAl catalysts

Malachite-like precursors in this study were obtained using a co-precipitation method at 60 °C and a pH of 7. Typically, 100 mL solution of metal nitrates was prepared such that (Cu + Zn + Zr + Al) metal concentration was 1 mol per liter. Metal nitrates salt solution and precipitating solution (1 M Na_2CO_3) were simultaneously added to a 100 mL DI water, separately heated in a 500 mL round flask at 60 °C, under vigorous stirring. The atomic ratio of Cu:Zn:Zr:Al was adjusted to be 6: 3.0-x: x:1 ($0.0 \leq x \leq 3.0$). Metal nitrate salt solution was added at 4 mL/min and the flow rate of precipitation solution was controlled to maintain the pH at around 7 during the precipitation. The resulting mixture was aged for 2 h under continuous stirring at 60 °C. CO_2 was bubbled through the mixture during aging and no pH rise was observed during the aging period [58]. Precipitates were separated via a vacuum filtration, washed with at least 2 liters of DI water and dried overnight under vacuum at 100 °C. The precursors of all compositions were calcined at 450 °C in air for 6 h with a ramp rate of 3 °C/min. The prepared catalysts were noted as $Cu_6Zn_{3.0-x}Zr_xAl_1$ where x = 0.0, 0.5, 1.5, 2.5, and 3.0. The compositions of metal oxides were measured by ICP-OES (iCAP 6000 Seires, Thermo, US).

2.2. Catalyst characterization of CuZnZrAl catalysts

Different characterization techniques were employed. X-ray diffraction measurements of the precursors and calcined catalysts were performed at room temperature with XRD-6000 diffractometer (Shimadzu Scientific Instruments, Japan) with Ni-filtered Cu-Kα (λ = 1.5418 Å) as a radiation source at scanning rate of $2^{\circ}\,min^{-1}$. The operating voltage and current were 35 kV and 40 mA, respectively. For analysis of the reduced catalysts, the reduced samples were taken after the reduction for 2 h at 250 °C. The samples were stored in Ar before the measure of XRD and TEM analysis. FT-IR spectra of catalyst precursors, vacuum dried at 100 °C overnight, were obtained with the spectrometer (iS10, Nicolet) equipped with a Smart iTR-ATR Sampling accessory.

High-resolution transmission electron microscopy (HRTEM) images were obtained with a TEM Titan microscope: FEI (Titan 80–300). The

TEM-Titan is operated at an accelerating voltage of 80–300 kV, an image resolution lower than 0.23 nm, an electon probe size smaller than 0.09 nm, the magnification of 25–1250000 X, and is equipped with Probe Cs corrector and Mono chromater. A high-angle annular dark-field scanning transmission electron microscopy (HAADF-STEM) and a TEM EDX (FEI (Talos F200 X)) were performed to get an insight into distribution of ZrO_2 aver Cu/ZnO islands. A TEM Talos is operated at an accelerating voltage of 80–200 kV, an image resolution of lower than 0.16, the magnification of 25-1500000X and Tomography holder angle ± 75°. The reduced samples were dispersed in acetone and the suspension was dropped to a TEM grid, which was dried for analysis. All post reduction steps were performed with a minimal air contact using glove box.

Cu-surface areas were determined with N_2O titration at atmospheric pressure using BELCAT-B catalyst analyzer (BEL, Japan Inc.) equipped with a thermal conductivity detector (TCD). Typically, 50 mg of catalyst was placed in a U-tube quartz reactor and reduced with 5% H_2 at 250 °C for 2 h. After the reduction, He was introduced into the reactor for 30 min at 250 °C to clean the reduced surface of catalyst. The reactor was subsequently cooled down to 90 °C in He, and then, was maintained at that temperature for 30 min in He. N_2O titration was performed after the detector signals were stabilized. N_2O pulses were injected and surface Cu only was oxidized (BELCAT-B). The surface oxidation of Cu takes place as follows [59]:

$$2Cu + N_2O \rightarrow Cu_2O + N_2$$

N_2O consumption at one pulse was used for the Cu surface area measurement. From the consumption of N_2O, Cu surface area was calculated using 1.47×10^{19} atoms of Cu/ m^2.

Temperature Programmed Reduction (TPR) of oxide catalysts was performed in the same equipment using 40 mg catalyst from room temperature to 400 °C (10 °C/min). TPR and in-situ XRD analysis of oxides catalysts under the H_2 reduction were performed to 750 °C and the experimental and results were described in SI.

Surface areas, pore volumes, and pore size distributions of the prepared samples were obtained from an N_2 physisorption analysis. The Brunauer-Emmett-Teller (BET) surface area measurements and N_2 adsorption-desorption measurements were performed at −196 °C using an automated gas sorption system (Belsorp II mini, BEL Japan, Inc.,). The Barrett–Joyner–Halenda (BJH) method was used for calculating pore size distribution. Each catalyst was degassed in vacuum at 200 °C for 3 h before the analysis.

2.3. Catalytic activity evaluation of CuZnZrAl catalysts

Methanol synthesis with the prepared catalysts was carried out in a continuous flow fixed bed reactor. 62.5 mg of oxide catalyst was loaded in a stainless steel tubular reactor (i.d.:3/8 in.), which was reduced at 250 °C for 3 h in 5% H_2/Ar gas (30 mL min^{-1}) under atmospheric pressure. After the reduction, the reactor was cooled to 200 °C and a mixture of H_2, CO and CO_2 gases was introduced into the reactor with a total flow rate of 200 mL min^{-1} and the pressure was increased to 40 atm using a back pressure valve, and then, methanol synthesis was performed at the different reaction temperatures. The effects of feed gas composition were investigated in the different feed composition of 100%, 50%, 20%, 10% and 5% CO_2 in carbon oxides at the fixed R ratio of 2. The R ratio is calculated as $(H_2 - CO_2)/(CO + CO_2)$. The products were analyzed using an on-line gas chromatograph (YL instruments 6500GC, S.Korea) equipped with a thermal conductivity detector (TCD) and flame Ionization Detector (FID) with a methanizer using a Carbosphere column. Products separated from the column were injected to the TCD detector first and the products from the TCD detector passed through the methanizer connected to the FID detector. Hydrogen (40 mL min^{-1}) was introduced into the methanizer connected to the FID detector. Gas products of CH_4, CO and CO_2 were quantified from the TCD detector and methanol was quantified from the FID detector with the reference of the methanized CO.

2.4. H/D exchange reaction on SiO_2

A 10% Cu/SiO_2 catalyst was prepared by an ammonia evaporation method. Typically, 22 g of $Cu(NO_3)_2.H_2O$ was dissolved in 100 mL of DI water in 500 mL beaker and 30% ammonia solution was added into it under vigorous stirring. When copper ammonia complex was formed at a high pH, 30 g of commercial SiO_2 (Sigma-Aldrich, Davisil, grade 633) was added into it. Mixture was stirred for about 30 min and then heated to 60 °C for evaporation of ammonia. When pH dropped to 7, Cu deposited SiO_2 was separated with filtration, dried overnight and calcined in air at 550 °C for 5 h. The 10 g of the calcined catalyst was reduced at 250 °C for 24 h in 5% H_2/Ar. Reduced catalysts was used for further studies.

ZnO was synthesized with a precipitation method. 100 mL of 1 M metalic salt solution of Zn nitrate salt and 1 M precipitating solution of Na_2CO_3 were simultaneously drop added into 100 mL DI water preheated at 60 °C under vigorous stirring. Flow rate of both solutions was adjusted such that the pH of precipitating mixture remained around 7. Resulting mixture was aged for about 3 h at 60 °C with CO_2 bubbling under constant stirring. Precipitates were separated by a filtration, dried at 90 °C overnight before the calcination at 350 °C for 6 h.

For in-situ FTIR measurements, catalyst slurries were prepared using ethanol and a thin layer of sample (around 4–7 mg) were deposited on CaF_2 window. All samples were pre-reduced in- situ before the H/D exchange reaction. The reduction was performed for 8 h in H_2 (60 mL min^{-1}), then purged for 3 h in He (60 mL min^{-1}) at 250 °C and a gas flow of 60 ml/min. The IR cell temperature was then cooled down to 125 °C and pressure was increased to 40 atm in He using a back pressure valve. Reference spectrum was collected before changing the He gas to D_2 (D_2:He = 3:1) gas at total flow of 60 ml/min. This reference spectrum was subtracted from all subsequent spectra obtained in the same experiment. Manual base line correction of the resultant spectra was obtained using an OMNIC software.

3. Results and discussions

3.1. Catalyst precursors

Fig. 1 shows XRD patterns of prepared dried precursors. The $Cu_6Zn_{0.0}Zr_{3.0}Al_1$ precursor without Zn shows a malachite structure, $Cu_2(OH)_2CO_3$ (JCPDS 41–1390). There are no Zr related phases in the XRD pattern of the $Cu_6Zn_{0.0}Zr_{3.0}Al_1$ precursor, indicating that the Zr component did not influence the precursor structure of the $Cu_6Zn_{0.0}Zr_{3.0}Al_1$ precursor. As the Zr content (x) is increased in the $Cu_6Zn_{3-x}Zr_xAl_1$ precursor, it was observed that the (20$\bar{1}$) and (21$\bar{1}$) peaks shifted to higher angles. However, the other reflections rarely

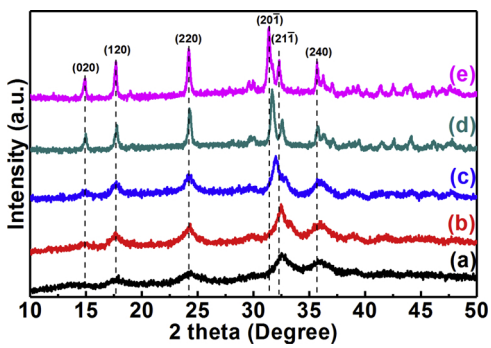

Fig. 1. XRD patterns of catalyst precursors dried at 100 °C overnight: (a) $Cu_6Zn_{3.0}Zr_{0.0}Al_1$ (b) $Cu_6Zn_{2.5}Zr_{0.5}Al_1$ (c) $Cu_6Zn_{1.5}Zr_{1.5}Al_1$ (d) $Cu_6Zn_{0.5}Zr_{2.5}Al_1$ and (e) $Cu_6Zn_{0.0}Zr_{3.0}Al_1$.

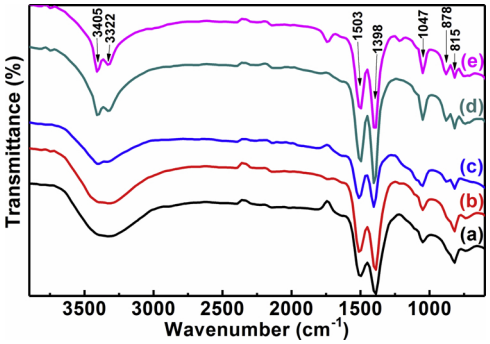

Fig. 2. FTIR spectra of catalyst precursors dried at 100 °C overnight: (a) $Cu_6Zn_{3.0}Zr_{0.0}Al_1$ (b) $Cu_6Zn_{2.5}Zr_{0.5}Al_1$ (c) $Cu_6Zn_{1.5}Zr_{1.5}Al_1$ (d) $Cu_6Zn_{0.5}Zr_{2.5}Al_1$ and (e) $Cu_6Zn_{0.0}Zr_{3.0}Al_1$.

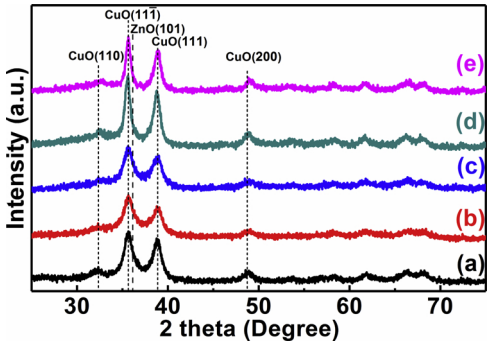

Fig. 3. XRD patterns of prepared oxide catalysts: (a) $Cu_6Zn_{3.0}Zr_{0.0}Al_1$ (b) $Cu_6Zn_{2.5}Zr_{0.5}Al_1$ (c) $Cu_6Zn_{1.5}Zr_{1.5}Al_1$ (d) $Cu_6Zn_{0.5}Zr_{2.5}Al_1$ and (e) $Cu_6Zn_{0.0}Zr_{3.0}Al_1$.

shifted. When the Zn content increased, the shifts of the angles at the (201) and (211) reflection is because Cu is gradually substituted by Zn. The Zn addition resulted in zincian malachite, $(Cu_{1-y}Zn_y)_2(OH)_2CO_3$, $0 < y < 3$) [60]. Here, no rosasite was observed, which can be observed at $y > 3$. The special sensitivity of the (201) and (211) peaks for the Zn substitution is pronounced, while the Zn substitution in malachite leads to a Vegard-type linear trend for all the lattice parameters of zincian malachite. This unusual behavior resulted from the Jahn-Teller effect, inducing that the lattice decreased as Cu was substituted by Zn (Table S1 and Fig. S1.). In the XRD analysis, it should be noted that Zr has no effects on the structure of precursors, again. The crystal sizes of $Cu_6Zn_{3.0}Zr_{0.0}Al_1$, $Cu_6Zn_{2.5}Zr_{0.5}Al_1$, $Cu_6Zn_{1.5}Zr_{1.5}Al_1$, $Cu_6Zn_{0.5}Zr_{2.5}Al_1$, and $Cu_6Zn_{0.0}Zr_{3.0}Al_1$ from the (220) reflections were 4.9, 9.5, 10.7, 30.6, and 29.5 nm, respectively. Crystal sizes of precursors were calculated by a Scherrer's equation. The crystal size of the precursors decreased with an increase in Zn content, which is also attributed to the Jahn-Teller effect.

Fig. 2 shows FTIR spectra of the precursors. The bands at 3405 and 3322 cm^{-1} of the $Cu_6Zn_{0.0}Zr_{3.0}Al_1$ precursor can be assigned to OH stretching modes of two crystallographically different OH ions present in the pure malachite crystal lattice [60,61]. These two bands became broader with an increase in Zn content of the CuZnZrAl precursor, until they were overlapped completely to make one broad band at around 3365 cm^{-1}. However, the bands at 1503 and 1398 cm^{-1} of the $Cu_6Zn_{0.0}Zr_{3.0}Al_1$ precursor, carbonate asymmetric stretching vibrational mode ($\nu 3$), did not shift as Cu was replaced by Zn in the malachite structure [59]. The bands at 878 and 1047 cm^{-1} can be assigned to M−OH bending modes [60,62] and the band at 815 cm^{-1} can be assigned to the carbonate out-of-plane bending mode ($\nu 2$). The intensity of M−OH bending mode decreased with increasing Zn content, while that of the carbonate out-of-plane bending mode rather increased.

3.2. Calcined catalysts

Fig. 3 shows XRD patterns of the calcined samples. Regardless of the composition of catalysts, only CuO peaks are present in all the prepared oxide catalysts. Absence of ZnO peak in Zn containing catalysts shows that ZnO is in amorphous phase and is well dispersed. ZrO_2 peaks are also not present in Zr containing samples, which indicates that ZrO_2 phase is also present in amorphous phase. $Cu_6Zn_{1.5}Zr_{1.5}Al_1$ shows the lowest crystal size of CuO among the prepared catalysts, although the crystal size of zincian malachite decreased with an increase of Zn. ZrO_2 may suppress the sintering of CuO by enclosing the zincian malachite. From these observations, it is proposed that the ZnO addition can enhance the dispersion of Cu by replacing Cu in the particles of malachite and ZrO_2 can prevent the sintering of CuO in the calcination step. The Zr addition has no effects in the zincian malachite formation, but it suppresses the CuO sintering in the calcination step.

Table 1 shows the physical properties of the prepared oxide catalysts. The BET surface area of the $Cu_6Zn_{1.5}Zr_{1.5}Al_1$ catalyst was the highest among the prepared oxide catalysts. BET surface area is in the order of $Cu_6Zn_{1.5}Zr_{1.5}Al_1 \approx Cu_6Zn_{2.5}Zr_{0.5}Al_1 > Cu_6Zn_{0.5}Zr_{2.5}Al_1 > Cu_6Zn_{0.0}Zr_{3.0}Al_1 > Cu_6Zn_3Zr_{0.0}Al_1$. The pore diameter of $Cu_6Zn_3Al_1$ and $Cu_6Zn_{1.5}Zr_{1.5}Al_1$ was the highest. When the prepared oxide catalysts were reduced, the crystal size the $Cu_6Zn_{1.5}Zr_{1.5}Al_1$ catalyst follows the order of CuO size.

Fig. 4 shows temperature programmed reduction (TPR) profiles of the prepared CuZnZrAl catalysts and Table 2 shows the amount of H_2 consumption in the TPR profiles. The reduction peaks correspond to the reduction of CuO. Two distinct peaks can be seen in all the profiles. The TPR patterns clearly show that the reduction curve at 225 °C becomes more distinctive as the content of Zr increases. The reduction curve at high temperature with $Cu_6Zn_{0.0}Zr_{3.0}Al_1$ (273 °C) was lower than that with $Cu_6Zn_{3.0}Zr_{0.0}Al_1$ (285 °C). Two different explanations in the literature about the reduction behavior of CuO were given to the TPR patterns of CuO. Two distinctive reduction peaks of CuO can be assigned to two step reduction of CuO: CuO→Cu_2O→Cu [63]. In the $Cu_6Zn_3Zr_{0.0}Al_1$, the second reduction step takes place immediately after the first reduction step, where two reduction peaks are not well distinguishable. However, the two peaks are separated more clearly with a decrease in the Zn/Zr atomic ratio: the second peak shifts to higher temperature and the second step is slightly delayed.

On the other hand, it was claimed that two types of CuO were present in all the catalysts showing different reduction behaviors: the amorphous CuO and crystalline CuO [64]. In the explanation, the first peak is assigned to the reduction of amorphous CuO and the second peak is to the reduction of the crystalline CuO. When we look at the XRD patterns in Fig. 3, the Cu crystal size increased with a decrease in the Zn/Zr ratio. However, the first peak rather increased with a decrease in ZnO content. Additionally, the separation of two peaks became more clear with increasing the CuO crystal size. When $Cu_6Zn_{3.0}Zr_{0.0}A_l$ (smaller Cu cryatal size) is compared with $Cu_6Zn_{0.0}Zr_{3.0}A1_1$ in the TPR patterns, the H_2 consumption in the first peak with $Cu_6Zn_{3.0}Zr_{0.0}A_l$ is much lower than that with $Cu_6Zn_{0.0}Zr_{3.0}A1_1$ (larger Cu crystal size). So, the second explanation is not applicable to the TPR patterns of the prepared Cu oxide catalysts. The H_2 consumption ratio of α to β with the Zr added catalysts increased with an increase in Zr content (CuO particle size). During the reduction of CuO/ZnO, it was observed that CuO was not fully reduced to Cu_2O in the first stage, but to Cu_2O/CuO [65] Therefore, the TPR pattern of the prepared Cu oxide samples are closely related to the crystal size of CuO and the reduction of CuO proceeds as CuO→Cu_2O/CuO →Cu. The first peak can be assigned to the reduction of CuO→Cu_2O/CuO. In-situ XRD and TPR analysis up to 750 °C was performed to monitor the reduction of CuO to Cu_2O/CuO and the structural changes as shown in Table S5, Fig. S4 and Fig. S5. The first step of CuO reduction is the reduction of CuO → CuO_2/CuO. And then, Cu_2O/CuO was reduced to Cu. Table S5 shows that the reduction of Cu_2O to

Table 1
Physical properties of prepared catalysts.

Catalysts	Oxide Catalyst				Reduced Catalyst	
	SA_{BET} ($m^2\,g^{-1}$)	Pore Size (nm)	Pore Vol. ($cm^3\,g^{-1}$)	CuO size[b](nm)	SA $_{Cu}$[a]($m^2\,g^{-1}$)	Cu size[b]from XRD (nm)
$Cu_6Zn_{3.0}Zr_{0.0}Al_1$	76	23.1	0.44	7.6	23.7	8.7
$Cu_6Zn_{2.5}Zr_{0.5}Al_1$	102	20.2	0.51	6.9	25.8	7.4
$Cu_6Zn_{1.5}Zr_{1.5}Al_1$	107	23.3	0.63	6.9	22.9	8.9
$Cu_6Zn_{0.5}Zr_{2.5}Al_1$	85	16.1	0.34	12.0	8.8	15.8
$Cu_6Zn_{0.0}Zr_{3.0}Al_1$	79	14.3	0.28	13.1	5.8	16.4

[a] Determined by N_2O titration.
[b] Calculated with Scherrer equation of 0.9 $\frac{\lambda}{\beta\cos\theta}$ (λ: 0.154 nm of CuK_α, β: FWHM (2θ)).

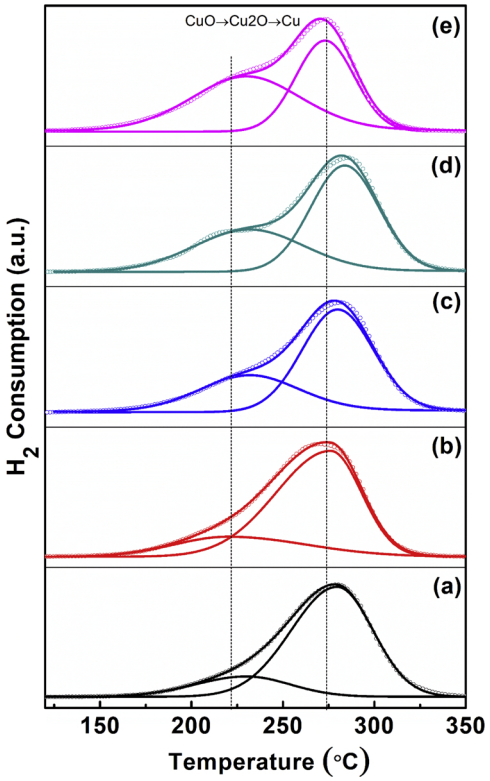

Fig. 4. TPR profiles of prepared catalysts: (a) $Cu_6Zn_{3.0}Zr_{0.0}Al_1$ (b) $Cu_6Zn_{2.5}Zr_{0.5}Al_1$ (c) $Cu_6Zn_{1.5}Zr_{1.5}Al_1$ (d) $Cu_6Zn_{0.5}Zr_{2.5}Al_1$ and (e) $Cu_6Zn_{0.0}Zr_{3.0}Al_1$.

Cu was the fastest on $Cu_6Zn_{0.0}Zr_{3.0}A_l$. The catalysts with the higher content ZnO was more resistant to the reduction of Cu_2O phase. The reduction of Cu_2O to Cu was the lowest on $Cu_6Zn_{1.5}Zr_{1.5}A_l$. The Cu sintering during the reduction was monitored by the measurement of Cu size (Fig. S5 and Table S7). It was observed that Cu sintering was also the lowest with $Cu_6Zn_{1.5}Zr_{1.5}A_l$.

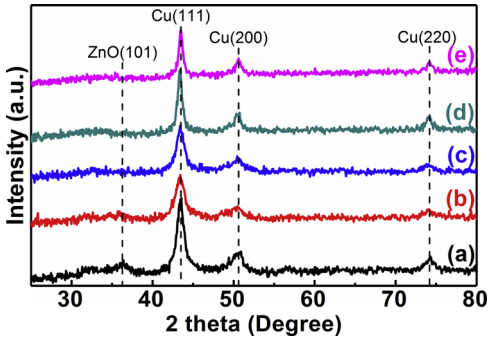

Fig. 5. XRD patterns of catalysts reduced for 2 h at 250 C using 5%H2/Ar gas: (a) $Cu_6Zn_3Zr_{0.0}Al_1$ (b) $Cu_6Zn_{2.5}Zr_{0.5}Al_1$ (c) $Cu_6Zn_{1.5}Zr_{1.5}Al_1$ (d) $Cu_6Zn_{0.5}Zr_{2.5}Al_1$ and (e) $Cu_6Zn_{0.0}Zr_{3.0}Al_1$.

3.3. Reduced catalyst

Fig. 5 shows XRD patterns of the reduced catalysts. The samples are taken for analysis after 2 h of reduction at the elevated temperature of 250 °C. As shown in Fig. 5, Cu characteristic peaks at 43.55°, 50.6° and 74.2° are assigned to (111), (200) and (220) planes, respectively. However, the peak at 36.28° is assigned to ZnO, which is slightly visible only with $Cu_6Zn_{3.0}Zr_{0.0}Al_1$. Therefore, ZnO can be considered very well dispersed after the reduction. Similarly, no ZrO_2 phase was detected in the reduced samples. The Cu crystal size of the reduced catalysts decreased with an increase in the Zn/Zr ratio, indicating the importance of ZnO for higher dispersion of Cu. The small Cu crystals resulted from the zincian malachite precursors of small crystal size. It should be noted that the Zr component has little effects on the structural changes in the zincian malachite formation, but it changes the structural changes during the calcination and the reduction steps.

Fig. 6 shows HAADF and TEM EDX mapping of the reduced $Cu_6Zn_{3.0}Zr_{0.0}Al_1$ (a1˜a4), $Cu_6Zn_{1.5}Zr_{1.5}Al_1$ (c1˜c5) and $Cu_6Zn_{0.0}Zr_{3.0}Al_1$ (e1˜e4) catalysts to examine the further insight into microstructure of the prepared samples. It is corresponding to the previous microstructure analysis of industrial $Cu/ZnO/Al_2O_3$ catalysts [66]. The TEM EDX mapping of $Cu_6Zn_{3.0}Zr_{0.0}Al_1$ shows that Cu and Zn particles are equally dispersed in $Cu_6Zn_{3.0}Zr_{0.0}Al_1$. However, Cu particles are agglomerated

Table 2
H_2 consumption of the prepared catalysts in Temperature Programmed Reduction (TPR).

Catalysts	Metal oxide composition (wt%)[a]				H_2 consumption (mmol/g_{cat})		
	CuO	ZnO	ZrO_2	Al_2O_3	α peak (225 °C)	β peak (275 °C)	Total
$Cu_6Zn_{3.0}Zr_{0.0}Al_1$	59.3	32.1	0.0	8.7	1.75	5.54	7.29
$Cu_6Zn_{2.5}Zr_{0.5}Al_1$	58.8	24.2	8.5	8.5	2.19	5.12	7.31
$Cu_6Zn_{1.5}Zr_{1.5}Al_1$	55.2	13.6	23.4	7.8	2.45	4.55	7.00
$Cu_6Zn_{0.5}Zr_{2.5}Al_1$	51.4	4.3	36.9	7.5	2.64	4.13	6.76
$Cu_6Zn_{0.0}Zr_{3.0}Al_1$	49.5	0.0	43.0	7.5	3.72	2.92	6.64

[a] Determined by I.C.P. analysis.

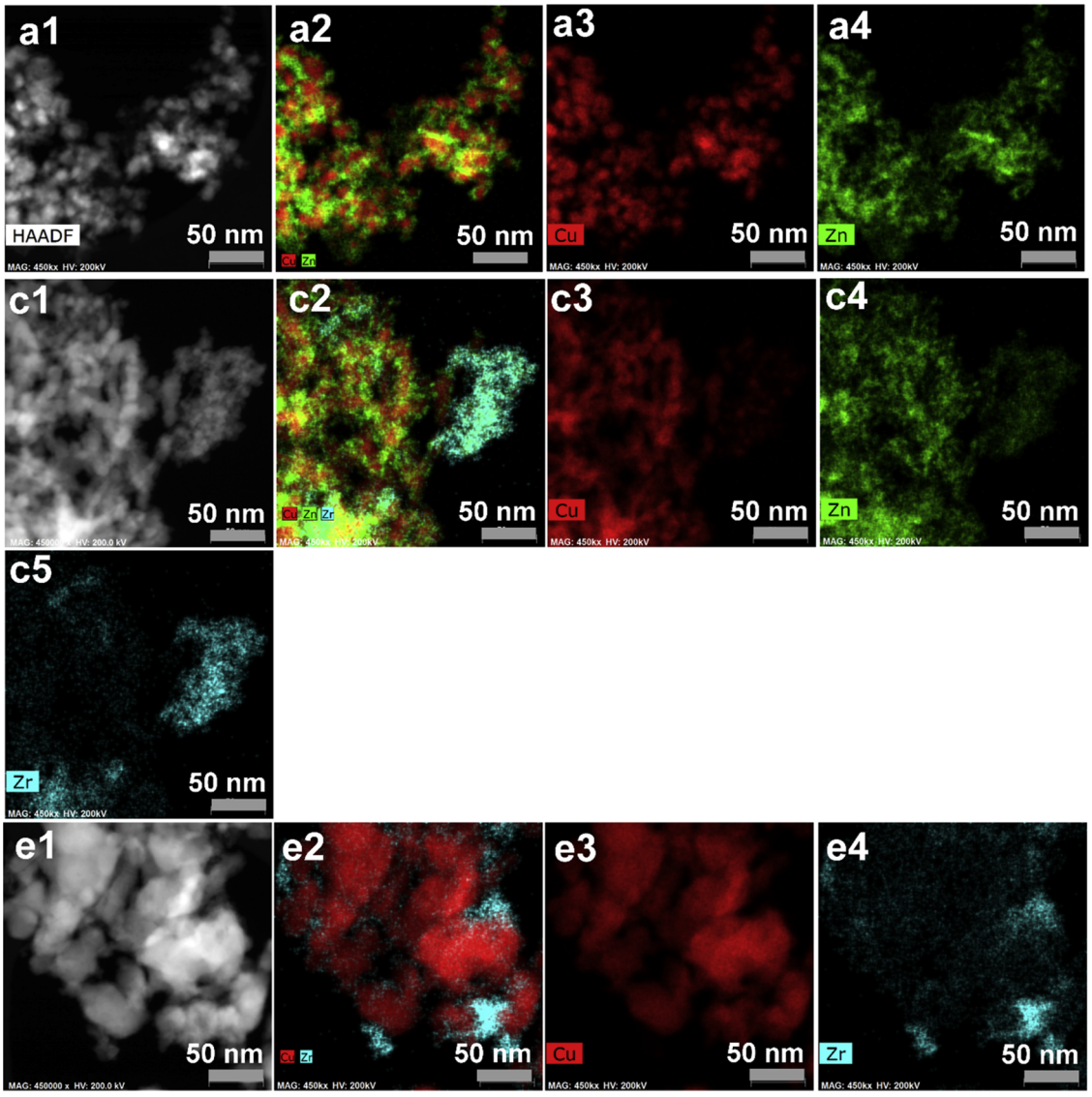

Fig. 6. HAADF and TEM EDX of $Cu_6Zn_{3.0}Zr_{0.0}Al_1$(a1– a4), $Cu_6Zn_{1.5}Zr_{1.5}Al_1$(c1– c4) and $Cu_6Zn_{0.0}Zr_{3.0}Al_1$ (e1– e4).

in the absence of ZnO in $Cu_6Zn_{0.0}Zr_{3.0}Al_1$(e1-e4). It is clear that the aggregated Cu particles are placed on ZrO_2 as shown in Fig. 6 (e1˜e4). The absence of ZrO_2 characteristic peaks in the XRD patterns (Figs. 3 and 5) is not due to the dispersed small ZrO_2 particles but to the amorphous phase of ZrO_2. The HAADF and TEM EDX analysis of $Cu_6Zn_{1.5}Zr_{1.5}Al_1$ and $Cu_6Zn_{0.0}Zr_{3.0}Al_1$ shows that Zr encloses $Cu_6Zn_{1.5}$ and Cu particles. Particle sizes of $Cu_6Zn_{3.0}Zr_{0.0}Al_1$, $Cu_6Zn_{1.5}Zr_{1.5}Al_1$ and $Cu_6Zn_{0.0}Zr_{3.0}Al_1$ (Table 1) are 8.7, 8.9 and 16.4 nm, respectively. It can be concluded that ZrO_2 was not dispersed near Cu and ZnO particles, but enclosed Cu/ZnO particles resulted from the zincian malachite particles.

It was claimed from TEM images on CuZnZr catalytic system that ZrO_2 was responsible to produce smaller Cu particles with increasing amount of ZrO_2 [65], suggesting that the CuZnZr catalysts were prepared by diluting Cu and ZnO with Zr. Therefore, in the previous report, the smaller Cu size was induced by the dilution of Zr. In our samples (Cu content in CuZnZrAl is fixed), the Cu size in the prepared CuZnZr catalyst can be decided mainly by the replacement of Cu by Zn. The amorphous Zr component encloses the zincian malachite in the preparation step of the precursors and Zr did not influence the precursor structures. ZrO_2 acts as suppressing the sintering of CuO in the calcination step only. Therefore, the smaller Cu sizes of $Cu_6Zn_{2.5}Zr_{0.5}Al_1$ and $Cu_6Zn_{1.5}Zr_{1.5}Al_1$ than that of $Cu_6Zn_{3.0}Zr_{0.0}Al_1$ are ascribed to the suppression of the CuO sintering in the calcination step. Similarly, the reduction of Cu_2O to Cu was the most retarded with $Cu_6Zn_{1.5}Zr_{1.5}Al_1$ as shown in Table S5. However, the replacement of Cu by Zn in malachite is also important step to disperse Cu. Further replacement of Zn by Zr (The Zn/Zr atomic ratio is less than 1.0) induced to increase the Cu particle size, because the increase of Cu size by the decrease of Zn overweighed the effect of ZrO_2 suppressing the CuO sintering in the calcination step. Therefore, it is concluded that the Cu size in CuZnZr can be decided mainly by ZnO content and ZrO_2 acts as a spacer to prevent the sintering of CuO in the calcination step. Similarly, ZrO_2 can act as a spacer to retard the reduction of Cu_2O to Cu in TPR (Fig. 4, Fig. S5 and Table S5). Fig.7 shows HRTEM analysis of the reduced $Cu_6Zn_{3.0}Zr_{0.0}Al_1$ (a1˜a3), $Cu_6Zn_{1.5}Zr_{1.5}Al_1$ (c1˜c3) and $Cu_6Zn_{0.0}Zr_{3.0}Al_1$ (e1˜e4) catalysts. During the sample preparation after the reduction, the outer phase of Cu is slightly oxidized showing the CuO/Cu_2O@Cu core-shell structure. Cu_2O@Cu phase was mainly observed on $Cu_6Zn_{0.0}Zr_{3.0}Al_1$. It was observed that ZnO was enclosed by CuO/Cu_2O@Cu on the samples of $Cu_6Zn_{3.0}Zr_{0.0}Al_1$ and $Cu_6Zn_{1.5}Zr_{1.5}Al_1$. It is clear that Cu/ZnO consists of the boundaries of Cu/Cu_2O and Cu/ZnO boundaries in Cu/ZnO particles. ZrO_2 encloses the Cu/ZnO particles resulted from zincian malachites. That kind of structure can stabilize

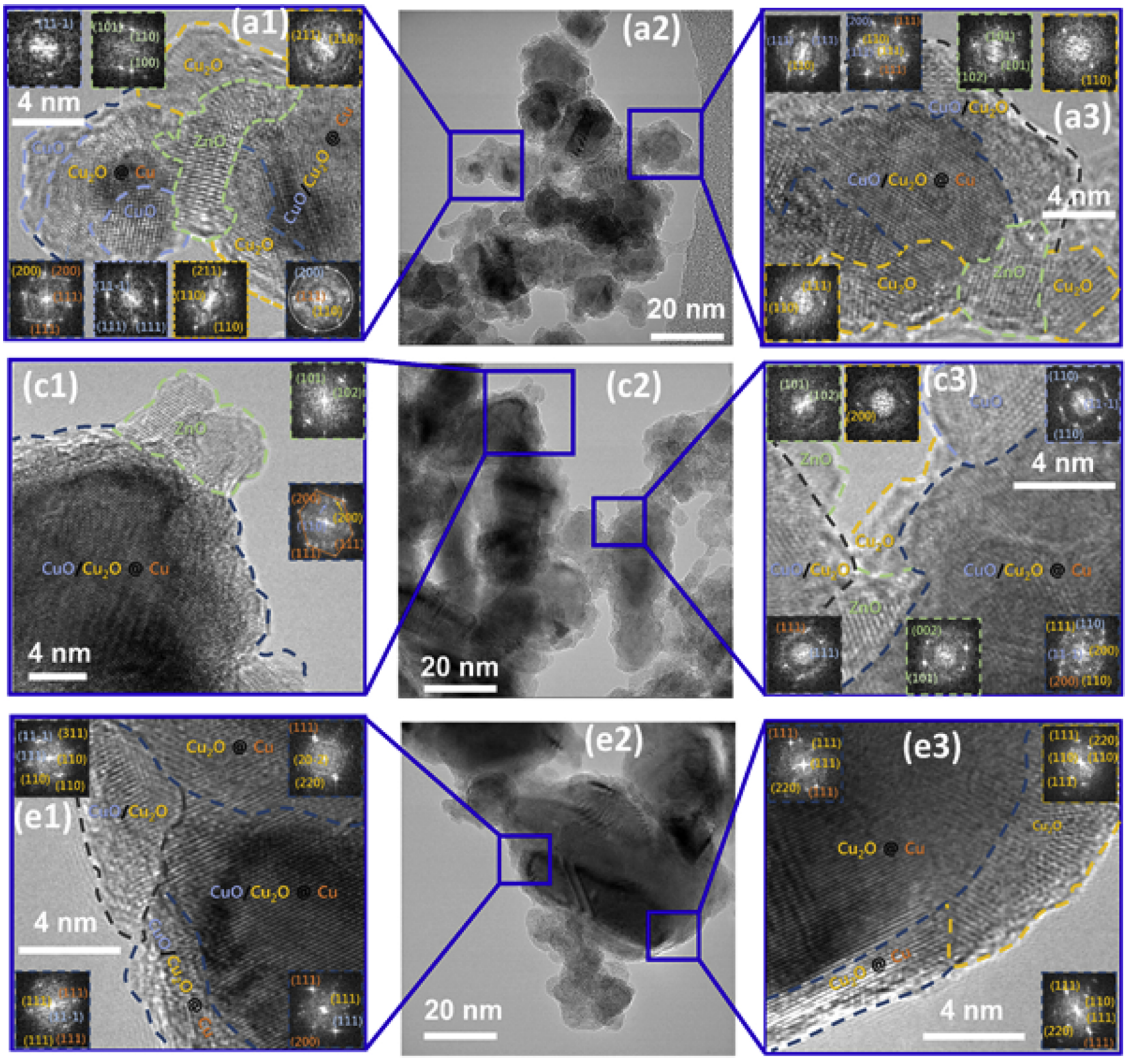

Fig. 7. HRTEM of $Cu_6Zn_{3.0}Zr_{0.0}Al_1$(a1– a3), $Cu_6Zn_{1.5}Zr_{1.5}Al_1$(c1– c3) and $Cu_6Zn_{0.0}Zr_{3.0}Al_1$ (e1– e3).

Cu/ZnO structurally.

3.4. Catalytic activity

It has been controversy that the ZrO_2 addition to $Cu_6Zn_3Al_1$ catalyst is effective on CO_2 hydrogenation. It was claimed that ZrO_2 could afford the additional active sites for CO_2 hydrogenation on $Cu/ZrO_2/SiO_2$ in CO_2 [67]. Here, methanol synthesis with the prepared CuZnZrAl catalysts was conducted in the wide range of feed composition of CO_2 at the fixed R ratio $((H_2-CO_2)/(CO+CO_2))$ of 2.0. To examine intrinsic activity, the catalytic reaction was performed at very high GHSV of 240,000 mL $g_{cat}^{-1}\,h^{-1}$.

Fig. 8. shows TOF (turnover frequency, s^{-1}, mol MeOH/molCu/s) values at 250 °C, 40 bar and a GHSV of 240,000 mL/gcat/h. The shift reaction is negligible at the high GHSV, because the compositions of CO and CO_2 in feed is similar to the ones in product (Table S2). The equilibrium constant (K_s) for shift reaction at 250 °C is 84.0. However, K values of shift reaction from the product stream at 240,000 mL g_{cat}^{-1} and 250 °C were 241, 209, 203, 494 and 1201 for $Cu_6Zn_{3.0}Zr_{0.0}Al_1$, $Cu_6Zn_{2.5}Zr_{0.5}Al_1$, $Cu_6Zn_{1.5}Zr_{1.5}Al_1$, $Cu_6Zn_{0.5}Zr_{2.5}Al_1$, $Cu_6Zn_0Zr_{3.0}Al_1$, respectively. Therefore, the obtained TOF values at the GHSV of 240,000 mL $g_{cat}^{-1}\,h^{-1}$ are mainly for CO/CO_2 hydrogenation to methanol. The TOF values increased with an increase in CO_2 composition in the feed at all the catalysts, agreeing on the previous results [15], suggesting that CO_2 is primary carbon source for methanol synthesis. It

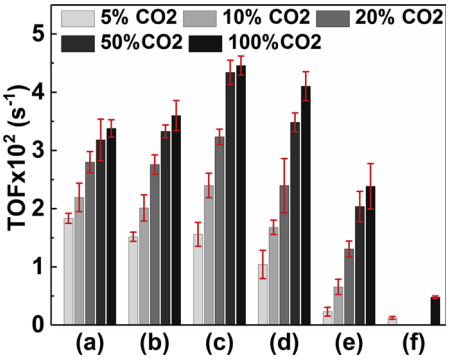

Fig. 8. Effect of CO_2 concentration in feed gas on Methanol TOF over prepared catalysts at 250 °C, 40 bar and 240,000 mL $gm_{cat}^{-1}\,h^{-1}$: (a) $Cu_6Zn_{3.0}Zr_{0.0}Al_1$ (b) $Cu_6Zn_{2.5}Zr_{0.5}Al_1$ (c) $Cu_6Zn_{1.5}Zr_{1.5}Al_1$ (d) $Cu_6Zn_{0.5}Zr_{2.5}Al_1$ (e) $Cu_6Zn_{0.0}Zr_{3.0}Al_1$ and (f) Cu_6Al_4.

was known that lower CO_2 content in feed shows higher methanol yield at the low GHSV, because of the high rate of shift reaction (Equilibrium is shifted by converting water, co-product with methanol, to H_2).

Alumina supported Cu catalyst (Cu_6Al_4) as a reference showed the lowest TOF even at much lower GHSV i.e. 96,000 mL $g_{cat}^{-1}\,h^{-1}$, indicating that alumina support has negligible effects on methanol synthesis. The TOF values in the 5% CO_2 feed increased with a decrease

in the x value of $Cu_6Zn_{3.0-x}Zr_xAl_1$ ($0 \le x \le 3$), while the ones with 50% and 100% CO_2 feed composition were maximized with $Cu_6Zn_{1.5}Zr_{1.5}Al_1$. TOF values in the 10% and 20% CO_2 feed are between ones in the 5% and 50% CO_2 feed. It should be noted that the TOF value of $Cu_6Zn_{0.5}Zr_{2.5}Al_1$ is higher than that of $Cu_6Zn_{3.0}Zr_{0.0}Al_1$ in 100% CO_2 feed. TOF is not dependent on the Cu size, if the Cu size is larger than 7.5 nm on the same supports [20], while TOF decreases with a decrease in Cu size if the Cu size was smaller than 7.5 nm. Therefore, the effect of the Cu size on TOF can be safely excluded in the prepared catalytic systems. TOF increased with an increase in the Zn/Zr ratio at the fixed Cu and Al composition in the 5% CO feed. On the other hand, the increase of the x value in $Cu_6Zn_{3.0-x}Zr_xAl_1$ increased TOF in the 100% CO_2 feed, maximizing TOF at $Cu_6Zn_{1.5}Zr_{1.5}Al_1$.

It should be mentioned that the role of ZnO on Cu/ZnO is not much different from the role of ZrO_2 on Cu/ZrO_2, emphasizing the bifunctionality of ZnO and ZrO_2 [46,49,50].

Reaction mechanism on Cu/MOx (MOx = ZnO or ZrO_2) in CO_2/H_2 and CO/H_2 is as follows:

CO_2/H_2 + Cu/MOx → Cu-formate and M-formate

CO/H_2 + Cu/MOx → M-formate (+ H_2O) only and no Cu-formate

Cu-formate/M-formate + 2 H_2 → M-methoxy + H_2O

M-formate without Cu → Zn-methoxy

M-methoxy + H_2O → CH_3OH + M − OH

Differently from ZnO, Zr-formate formed via hydrogenation of Zr-hydroxycarbonate in CO_2, while Zr-formate formed by the CO insertion into Zr − OH in the CO feed. On the other hand, it was claimed that ZnO can act as a reservoir of H atoms, which can migrate to other sites [68], but it was not observed that ZrO_2 could afford the reservoir of H atoms.

There were no ZrO_2 additional effects in methanol synthesis in 5% CO. Excess CO is inserted into Zr − OH to form Zr-formate depleting surface hydroxyls on ZrO_2. The migration of hydrogen for hydrogenation can be blocked due to the depleting surface hydroxyls. It was observed that the hydrogen spillover was blocked on the Zr-formate prepared from the CO insertion into Zr − OH [49]. On the other hand, the capability of reverse spillover of ZnO can facilitate the hydrogenation of Zn-formate even in 5% CO [46,68]. The TOF ratios of $(TOF)_{5\%CO2}/(TOF)_{100\%CO2}$ were 1.8 for $Cu_6Zn_{3.0}Zr_{0.0}Al_1$ and 10.4 for $Cu_6Zn_{0.0}Zr_{3.0}Al_1$, which indicates that ZrO_2 can play an important role only in the high CO_2 feed.

Surface hydroxyls can facilitate hydrogen spillover from Cu to ZrO_2, although it suppresses methanol synthesis near equilibrium conversion. It was reported that surface hydroxyls facilitated hydrogen spillover on Cu/ZrO_2 [49] and Pt/silica-alumina [56]. In 100% CO_2 feed, water and Zr − OH can be produced in the hydrogenation steps of Zr-hydroxycarbonate and Zr-formate and the produced Zr − OH on the surface of catalysts can play a role of the enhancement of hydrogen spillover and hydrolysis. In the 100% CO_2 feed, surface hydroxyls were produced with Zr-methoxy from hydrogenation of Zr-hydroxycarbonate and Zr-formate. Furthermore, the reverse spillover from Cu/ZnO can facilitate hydrogenation on Cu/ZrO. Therefore, the synergistic effect of ZnO (reverse spillover) and ZrO_2 (bifuntionality) on $Cu_6Zn_{1.5}Zr_{1.5}Al_1$ were pronounced for methanol synthesis in 100% CO_2 feed, but the role of ZrO2 was suppressed in 5% CO_2 feed.

If the reverse spillover is valid in CO_2 hydrogenation on CuZnZrAl catalytic system, it can deduce that the role of ZrO_2 to afford additional active sites can be more pronounced in the presence of ZnO. Then, the reason of high activity of $Cu_6Zn_{0.5}Zr_{2.5}Al_1$ as well as $Cu_6Zn_{1.5}Zr_{1.5}Al_1$ can be due to both the hydrogen spillover from Cu to ZrO_2 and the reverse hydrogen spillover from Cu/ZnO to ZrO_2 in CO_2 hydrogenation, because ZrO_2 requires spilt hydrogen for CO_2 hydrogenation.

3.5. Reverse hydrogen spillover from ZnO via Cu

For the confirmation of reverse hydrogen spillover of ZnO, four samples of SiO_2, Zn/SiO_2(B), Cu/SiO_2, and Cu/ZnO/SiO_2 are prepared for H/D exchange reaction. Fig. 9 shows the H/D exchange rates from

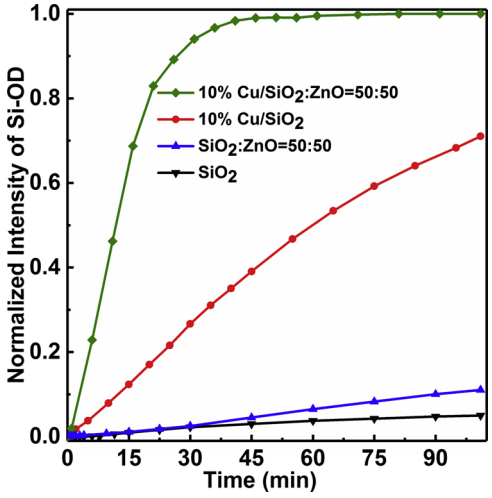

Fig. 9. Intensity of OD-Si during exposure of samples in (D_2:He = 3:1) at a total D_2/He flow rates of 60 ml/min at 125 °C and 40 atm.

IR spectra during the exchange of Si—OH by Si—OD at 125 °C and 40 atm (Fig. S2). Si—OH is transformed to Si—OH by exchanging H_2 gas with D_2 gas. When ZnO was physically added to SiO_2 by kneadding, the exchange reaction increased a little. When Cu was added to SiO_2, the H/D exchange reaction rate was significantly increased, which can be ascribed to the hydrogen spillover from Cu to SiO_2 as observed in Cu/ZrO_2 system [49,69]. When ZnO was added to Cu/SiO_2, the exchange reaction rate was further two times more increased. As shown in SiO_2 and ZnO/SiO_2, it can be deduced that ZnO has low capability of H_2 dissociation. So, it is reasonable that ZnO has a reservoir to keep spilt hydrogen and the fast exchange reaction can be due to the reverse spillover of spilt hydrogen supplied from Cu supporting the previous results from TPD analysis [47,68]. Here, the H/D exchange reaction was supplemented for the reverse spillover as a reason of the synergistic effect of Cu and ZnO. The H/D exchange for the hydrogen spillover has been ongoing debates, suggesting that the hydrogen spillover from metal to nonreducible oxide is not facile [54]. However, recent rigorous experiments and theoretical calculation exhibited that hydrogen spillover from metal to nonreducible oxide was facile via surface hydroxyls [55,57,69], Methanol synthesis over Cu/SiO_2 and Cu/ZnO/SiO_2 was performed to correlate the activity with the H/D exchange as shown in Fig.10. TOF increased almost 2 times with physical mixing of ZnO with the Cu/SiO_2 catalyst. When a small amount of ZnO was added to Cu/ZrO_2, the TOF value increased two times from 0.024 s^{-1} for $Cu_6Zn_{0.0}Zr_{3.0}Al_1$ from 0.043 s^{-1} for $Cu_6Zn_{0.5}Zr_{2.5}Al_1$. The TOF increase with the ZnO addition to the Cu/ZrO_2 is attributed to the role of reverse spillover of Cu/ZnO to ZrO_2 in 100% CO_2.

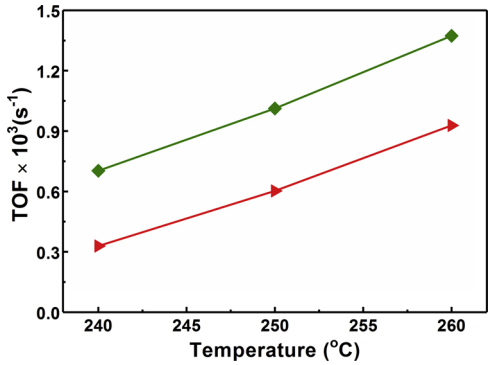

Fig. 10. Effect of ZnO physical mixing on TOF of the methanol synthesis from CO_2 hydrogenation at 40 atm pressure and 2500 mL g_{cat}^{-1} h^{-1}. (◆)10%Cu/SiO_2:ZnO = 50:50 (w/w) (▶)10%Cu/SiO_2:Innert(Corundum) = 50:50 (w/w).

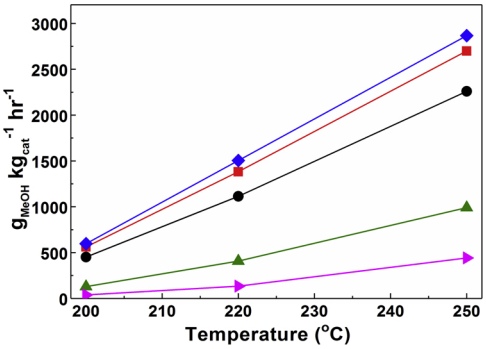

Fig. 11. Methanol productivity for CO_2 hydrogenation over prepared catalysts at 250 °C, 40 bar and 240,000 mL gm_{cat}^{-1} h^{-1}: (●) $Cu_6Zn_3Zr_{0.0}Al_1$ (■) $Cu_6Zn_{2.5}Zr_{0.5}Al_1$ (◆) $Cu_6Zn_{1.5}Zr_{1.5}Al_1$ (▲) $Cu_6Zn_{0.5}Zr_{2.5}Al_1$ and (▶) $Cu_6Zn_{0.0}Zr_{3.0}Al_1$.

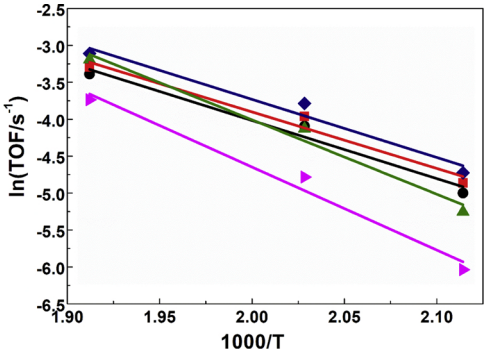

Fig. 12. Arrhenius plot of (●) $Cu_6Zn_3Zr_{0.0}Al_1$ (■) $Cu_6Zn_{2.5}Zr_{0.5}Al_1$ (◆) $Cu_6Zn_{1.5}Zr_{1.5}Al_1$ (▲) $Cu_6Zn_{0.5}Zr_{2.5}Al_1$ and (▶) $Cu_6Zn_{0.0}Zr_{3.0}Al_1$ catalysts at 40 bar and 240,000 mL g_{cat} h^{-1}.

Fig. 11 shows the methanol productivity of the prepared catalysts at the different reaction temperature. The $Cu_6Zn_{1.5}Zr_{1.}5Al1$ catalyst exhibits the highest productivity as well as the highest TOF. The carbon balance and methanol selectivity at 240,000 mL g_{cat} h^{-1} were listed in Table S3. Methanol selectivity in CO_2 hydrogenation was also the highest on $Cu_6Zn_{1.5}Zr_{1.5}Al_1$. The performances of the other reported catalytic system are listed for comparison with this report in Table S4. Recently, kinetic equation was derived using Cu/Zn/Zr/Al catalytic system [70]. The result (491 g MeOH kg_{cat} h^{-1}) using the kinetic equation at 250 °C and a GHSV of 10,000 mL g_{cat} h^{-1} gave the similar performance to this report (489 g MeOH kg_{cat} h^{-1}) with $Cu_6Zn_{1.5}Zr_{1.5}Al_1$ at the same reaction condition. The apparent activation energies of the prepared catalysts were obtained as shown in Fig. 12 and Table 3. The apparent activation was obtained by Arrhenius plot of ln(TOF) vs 1/T at GHSV 240,000 mL g_{cat}^{-1} h^{-1} for CO_2 hydrogenation to methanol. The apparent activation energies of $Cu_6Zn_3Zr_{0.0}Al_1$, $Cu_6Zn_{2.5}Zr_{0.5}Al_1$, $Cu_6Zn_{1.5}Zr_{1.5}Al_1$, $Cu_6Zn_{0.5}Zr_{2.5}Al_1$ and $Cu_6Zn_{0.0}Zr_{3.0}Al_1$ were 65.39, 63.61, 65.41, 83.73 and 93.46 kJ mol^{-1}, respectively. The apparent activation energy of $Cu_6Zn_{3.0}Zr_{0.0}Al_1$ was not much changed until x in $Cu_6Zn_{3-x}Zr_xAl_1$ became 1.5. However, the further increase of x value in $Cu_6Zn_{3-x}Zr_xAl_1$ increased the apparent activation energy a lot. It was reported that Cu/ZnO catalysts had the apparent activation energy of ca. 57 kJ mol^{-1} [71], which was a little higher than the value in this report. The apparent activation energy increased with a Zr content and the CuZnZr (32/24/44) catalyst showed the activation energy of 66 kJ/mol. The apparent activation energy of Cu/ZrO_2 was reported 97 kJ mol^{-1} [72], which was similar to the value in this report.

4. Conclusion

TOF increased with an increase in CO_2 content of the carbon oxide feed on the all the prepared CuZnZrAl catalysts indicating that CO_2 is primary carbon source for methanol synthesis. The bifunctionality of ZnO and ZrO_2 on Cu/ZnO and Cu/ZrO_2 suggested the similar reaction path for methanol synthesis [35–37,39–41,46,47,49,63,64]: CO_2/H_2 → Cu-formate/Zn-formate/Zr-formate (+H_2) → Zn-methoxy/Zr-methoxy (+H_2O) → methanol. However, the TOF ratios of $(TOF)_{5\%CO2}/(TOF)_{100\%CO2}$ in the feed with the different CO_2 composition were 1.8 for $Cu_6Zn_{3.0}Zr_{0.0}Al_1$ and 10.4 for $Cu_6Zn_{0.0}Zr_{3.0}Al_1$, respectively (Fig. 8). The large different $(TOF)_{5\%CO2}/(TOF)_{100\%CO2}$ over $Cu_6Zn_{0.0}Zr_{3.0}Al_1$ indicates that the role of ZrO_2 is predominant only in 100 % CO_2 feed as compared with $Cu_6Zn_{3.0}Zr_{0.0}Al_1$. The structural effect of ZrO_2 was observed to suppress the sintering of Cu and to retard the reduction of Cu_2O to Cu by in-situ XRD and TPR analysis. However, the structural effect to stabilize Cu/Cu^{+1} should be retained irrespective of the feed composition of CO and CO_2, but the kinetic data exhibited that the effect of ZrO_2 on Cu/ZnO was pronounced only in CO_2 rich feeds. Therefore, the structural effect of ZrO_2 to stabilize Cu/Cu^{+1} may not be important factor for the intrinsic activity of methanol synthesis. On the other hand, it was observed the reverse spillover of ZnO from the H/D exchange reaction (Fig. 9) and the capability of the reverse spillover of ZnO can differentiate the role of ZnO from the one of ZrO_2. The Zr−OH plays a role in methanol synthesis on Cu/ZrO_2 in CO_2/H_2, but it has no capability as hydrogen reservoir like ZnO. Methanol is produced in CO_2/H_2 on ZrO_2 by a little different reaction sequences from that on ZnO: Zr−OH (+ CO_2) → Zr−OCOOH (+H_2) → Zr−OCHO (+H_2) → Zr−OCH_3 (+H_2O) → CH_3OH + Zr−OH. Hydroxyls can facilitate the migration of hydrogen on ZrO_2 [47,50]. On the other hand, the migration of hydrogen in CO/H_2 is not facile on ZrO_2, because CO is inserted into Zr−OH to form Zr-formate directly depleting the surface hydroxyls. Therefore, the migration of hydrogen can be hindered on Cu/ZrO_2 in the CO-rich feed (5% CO_2), while it is not much hindered on $Cu/ZnO/ZrO_2$ due to the capability of reverse spillover of ZnO even in the CO-rich feed (5% CO_2). Therefore, it can be concluded that the role of ZrO_2 can be responsible for methanol synthesis in the CO_2/H_2 feed only. From theses observation, $Cu_6Zn_{1.5}Zr_{1.5}Al_1$ showed the highest TOF. The hydrogen spillover from Cu and the reverse hydrogen spillover from ZnO enhanced methanol synthesis on ZrO_2 over $Cu_6Zn_{1.5}Zr_{1.5}Al_1$ in 100% CO_2.

Table 3
The apparent activation energies (kJ/mol) of prepared catalysts at 40 bar and 240,000 mL g_{cat}^{-1} h^{-1}.

$Cu_6Zn_{3.0}Zr_{0.0}Al_1$	$Cu_6Zn_{2.5}Zr_{0.5}Al_1$	$Cu_6Zn_{1.5}Zr_{1.5}Al_1$	$Cu_6Zn_{0.5}Zr_{2.5}Al_1$	$Cu_6Zn_{0.0}Zr_{3.0}Al_1$
65.4	63.6	63.4	83.7	93.5

Acknowlegements

This work was supported by Next Generation Carbon Upcycling Project"(Project No. 2017M1A2A2043134) through the National Research Foundation (NRF) funded by the Ministry of Science and ICT, Republic of Korea and by Korea Institute of Science and Technology. We thank to Dr. Sung Chul Kim for the in-situ XRD analysis.

Appendix A. Supplementary data

Supplementary material related to this article can be found, in the online version, at doi:https://doi.org/10.1016/j.apcatb.2019.117971.

References

[1] M. Alvarado, Methanol Industry Overview, Stanford Methanol Meet, (2017).
[2] The Tight Link Between Methanol and Olefins, IHS Markit, 2018, https://cdn.ihs.com/www/blog/20180411-Chem-MTO-Infographic.pdf.
[3] J.M. Ogden, Hydrogen: The Fuel of the Future? Phys. Today 55 (2002) 69–75, https://doi.org/10.1063/1.1480785.
[4] D. Cardenas, Methanol and Hydrogen Production: Energy and Cost Analysis, Master's Thesis, Lulea U. of Technology, 2006, pp. 1–57 ISSN:1653-0187.
[5] G.K.S.P. George, A. Olah, Alain Goeppert, Beyond Oil and Gas: the Methanol Economy, 3rd editio, (2006), https://doi.org/10.1016/S1351-4180(06)71901-8.
[6] M. Behrens, Chemical hydrogen storage by methanol: challenges for the catalytic methanol synthesis from CO_2, Recycl. Catal. 2 (2015) 78–86, https://doi.org/10.1515/recat-2015-0009.
[7] M. O'Neil, The Merck Index - an Encyclopedia of Chemicals, Drugs, and Biologicals, 13th edition, 15th editi, Royal Society of Chemistry, Cambridge, UK, 2013.
[8] S. Lee, J.G. Speight, S.K. Loyalka, Handbook of Alternative Fuel Technologies, (2015), https://doi.org/10.1039/b702989f.
[9] K. Roh, T.B.H. Nguyen, U. Suriyapraphadilok, J.H. Lee, R. Gani, Development of sustainable CO2 conversion processes for the methanol production, Comput. Aided Process Eng. 37 (2015) 1145–1150, https://doi.org/10.1016/B978-0-444-63577-8.50036-X.
[10] A. Baiker, Utilization of carbon dioxide in heterogeneous catalytic synthesis, Appl. Organomet. Chem. 14 (2000) 751–762, https://doi.org/10.1002/1099-0739(200012)14:12<751::AID-AOC85>3.0.CO;2-J.
[11] Peter Davies; F. F. Snowdon; G. W. Bridger; D. O. Huges; P. W. Young, GB Patent, 1 296 212, assigned to ICI, 1961.
[12] G.C. Chinchen, P.J. Denny, D.G. Parker, M.S. Spencer, D.A. Whan, Mechanism of methanol synthesis from CO2/CO/H2 mixtures over copper/zinc oxide/alumina catalysts: use of 14C-labelled reactants, Appl. Catal. 30 (1987) 333–338, https://doi.org/10.1016/S0166-9834(00)84123-8.
[13] M. Behrens, F. Studt, I. Kasatkin, S. Kühl, M. Hävecker, F. Abild-Pedersen, S. Zander, F. Girgsdies, P. Kurr, B.-L. Kniep, M. Tovar, R.W. Fischer, J.K. Nørskov, R. Schlögl, The active site of methanol synthesis over $Cu/ZnO/Al_2O_3$ industrial catalysts, Science 336 (2012) 893–897, https://doi.org/10.1126/science.1219831.
[14] A. Le Valant, C. Comminges, C. Tisseraud, C. Canaff, L. Pinard, Y. Pouilloux, The Cu-ZnO synergy in methanol synthesis from CO_2, Part 1: origin of active site explained by experimental studies and a sphere contact quantification model on Cu + ZnO mechanical mixtures, J. Catal. 324 (2015) 41–49, https://doi.org/10.1016/j.jcat.2015.01.021.
[15] F. Studt, M. Behrens, E.L. Kunkes, N. Thomas, S. Zander, A. Tarasov, J. Schumann, E. Frei, J.B. Varley, F. Abild-Pedersen, J.K. Nørskov, R. Schlögl, The mechanism of CO and CO2 hydrogenation to methanol over Cu-based catalysts, ChemCatChem 7 (2015) 1105–1111, https://doi.org/10.1002/cctc.201500123.
[16] C.E. Pompe, M. Slagter, P.E. de Jongh, K.P. de Jong, Impact of heterogeneities in silica-supported copper catalysts on their stability for methanol synthesis, J. Catal. Submitt. 365 (2018) 1–9, https://doi.org/10.1016/j.jcat.2018.06.014.
[17] B. Hu, Y. Yin, G. Liu, S. Chen, X. Hong, S.C.E. Tsang, Hydrogen spillover enabled active Cu sites for methanol synthesis from CO2hydrogenation over Pd doped CuZn catalysts, J. Catal. 359 (2018) 17–26, https://doi.org/10.1016/j.jcat.2017.12.029.
[18] C. Tisseraud, C. Comminges, T. Belin, H. Ahouari, A. Soualah, Y. Pouilloux, A. Le Valant, The Cu-ZnO synergy in methanol synthesis from CO2, Part 2: origin of the methanol and CO selectivities explained by experimental studies and a sphere contact quantification model in randomly packed binary mixtures on Cu-ZnO co-precipitate catalysts, J. Catal. 330 (2015) 533–544, https://doi.org/10.1016/j.jcat.2015.04.035.
[19] C. Tisseraud, C. Comminges, S. Pronier, Y. Pouilloux, A. Le Valant, The Cu–ZnO synergy in methanol synthesis Part 3: Impact of the composition of a selective Cu@ZnOxcore–shell catalyst on methanol rate explained by experimental studies and a concentric spheres model, J. Catal. 343 (2016) 106–114, https://doi.org/10.1016/j.jcat.2015.12.005.
[20] R. van den Berg, G. Prieto, G. Korpershoek, L.I. van der Wal, A.J. van Bunningen, S. Lægsgaard-Jørgensen, P.E. de Jongh, K.P. de Jong, Structure sensitivity of Cu and CuZn catalysts relevant to industrial methanol synthesis, Nat. Commun. 7 (2016) 13057, https://doi.org/10.1038/ncomms13057https://www.nature.com/articles/ncomms13057#supplementary-information.
[21] K. Larmier, W.-C. Liao, S. Tada, E. Lam, R. Verel, A. Bansode, A. Urakawa, A. Comas-Vives, C. Copéret, CO2-to-Methanol hydrogenation on zirconia-supported copper nanoparticles: reaction intermediates and the role of the metal–support interface, Angew. Chemie Int. Ed. 56 (2017) 2318–2323, https://doi.org/10.1002/anie.201610166.
[22] S. Kattel, P.J. Ramírez, J.G. Chen, J.A. Rodriguez, P. Liu, Active sites for CO2 hydrogenation to methanol on Cu/ZnO catalysts, Science 355 (2017) 1296–1299, https://doi.org/10.1126/science.aal3573.
[23] B. Yang, C. Liu, A. Halder, E.C. Tyo, A.B.F. Martinson, S. Seifert, P. Zapol, L.A. Curtiss, S. Vajda, Copper cluster size effect in methanol synthesis from CO_2, J. Phys. Chem. C. 121 (2017) 10406–10412, https://doi.org/10.1021/acs.jpcc.7b01835.
[24] C. Tisseraud, C. Comminges, A. Habrioux, S. Pronier, Y. Pouilloux, A. Le Valant, Cu-ZnO catalysts for CO2hydrogenation to methanol: morphology change induced by ZnO lixiviation and its impact on the active phase formation, Mol. Catal. 446 (2018) 98–105, https://doi.org/10.1016/j.mcat.2017.12.036.
[25] R.M. Palomino, P.J. Ramírez, Z. Liu, R. Hamlyn, I. Waluyo, M. Mahapatra, I. Orozco, A. Hunt, J.P. Simonovis, S.D. Senanayake, J.A. Rodriguez, Hydrogenation of CO2on ZnO/Cu(100) and ZnO/Cu(111) catalysts: role of copper structure and metal-oxide interface in methanol synthesis, J. Phys. Chem. B 122 (2018) 794–800, https://doi.org/10.1021/acs.jpcb.7b06901.
[26] K. Klier, Methanol synthesis, J. Adv. Catal. Sci. Technol. 31 (1982) 243–313, https://doi.org/10.1016/S0360-0564(08)60455-1.
[27] A. Rozovskii, No Title, React. Kinet. Catal. Lett. 21 (1980) 97.
[28] J.B. Hansen, E.P.H. Nielsen, Methanol synthesis, in: G. Ertl, H. Knözinger, F. Schüth, J. Weitkamp (Eds.), Handb. Heterog. Catal, Wiley-VCH Verlag GmbH & Co. KGaA, Weinheim, Germany, 2006, pp. 2920–2949.
[29] J. Szanyi, D.W. Goodman, Methanol synthesis on a Cu(100) catalyst, Catal. Lett. 10 (1991) 383–390, https://doi.org/10.1007/BF00769173.
[30] K.C. Waugh, Methanol synthesis, Catal. Today 15 (1992) 51–75, https://doi.org/10.1016/0920-5861.
[31] P. Rasmussen, P. Holmblad, T. Askgaard, Methanol synthesis on Cu (100) from a binary gas mixture of CO_2 and H_2, Catal. Lett. 26 (1994) 373, https://doi.org/10.1007/BF00810611.
[32] P.B. Rasmussen, M. Kazuta, I. Chorkendorff, Synthesis of methanol from a mixture of H2 and CO_2 on Cu(100), Surf. Sci. 318 (1994) 267–280, https://doi.org/10.1016/0039-6028(94)90101-5.
[33] J. Yoshihara, C.T. Campbell, Methanol synthesis and reverse water-gas shift kinetics over Cu(110) model catalysts: structural sensitivity, J. Catal. 161 (1996) 776–782, https://doi.org/10.1006/jcat.1996.0240.
[34] J. Yoshihara, S.C. Parker, A. Schafer, C.T. Campbell, Methanol synthesis and reverse water-gas shift kinetics over clean polycrystalline copper, Catal. Lett. 31 (1995) 313–324, https://doi.org/10.1007/BF00808595.
[35] T. Fujitani, I. Nakamura, T. Watanabe, T. Uchijima, J. Nakamura, Methanol synthesis by the hydrogenation of CO_2 over Zn-deposited Cu(111) and Cu(110) surfaces, Catal. Lett. 35 (1995) 297–302, https://doi.org/10.1007/BF00807186.
[36] T. Fujitani, I. Nakamura, T. Uchijima, J. Nakamura, The kinetics and mechanism of methanol synthesis by hydrogenation of CO_2 over a Zn-deposited Cu(111) surface, Surf. Sci. 383 (1997) 285–298, https://doi.org/10.1016/S0039-6028(97)00192-1.
[37] G.C. Chinchen, K.C. Waugh, D.A. Whan, The activity and state of the copper surface in methanol synthesis catalysts, Appl. Catal. Appl. Catal. 25 (1986) 101–107, https://doi.org/10.1016/s0166-9834(00)81226-9.
[38] P.L. Hansen, Atom-resolved imaging of dynamic shape changes in supported copper nanocrystals, Science 295 (2002) 2053–2055, https://doi.org/10.1126/science.1069325.
[39] R. Burch, R.J. Chappell, S.E. Golunski, Synergy between copper and zinc oxide during methanol synthesis. Transfer of activating species, J. Chem. Soc. Faraday Transl. Phys. Chem. Condens. Phases. 85 (1989) 3569, https://doi.org/10.1039/f19898503569.
[40] O.S. Joo, K.D. Jung, S.H. Han, S.J. Uhm, D.K. Lee, S.K. Ihm, Migration and reduction of formate to form methanol on Cu/ZnO catalysts, Appl. Catal. A Gen. 135 (1996) 273–286, https://doi.org/10.1016/0926-860X(95)00256-1.
[41] M.S. Spencer, Role of ZnO in methanol synthesis on copper catalysts, Catal. Lett. 50 (1998) 37–40, https://doi.org/10.1023/A:1019098414820.
[42] J. Graciani, K. Mudiyanselage, F. Xu, A.E. Baber, J. Evans, S.D. Senanayake, D.J. Stacchiola, P. Liu, J. Hrbek, J.F. Sanz, J.A. Rodriguez, Highly active copper-ceria and copper-ceria-titania catalysts for methanol synthesis from CO_2, Science 345 (2014) 546–550, https://doi.org/10.1126/science.1253057.
[43] X. Fang, Y. Men, F. Wu, Q. Zhao, R. SIngh, P. Xiao, T. Du, P.A. Webley, Improved methanol yield and selectivity from CO2 hydrogenation using a novel Cu-ZnO-ZrO2 catalyst supported on Mg-Al layered double hydroxide(LDH), J. CO2 Util. (2019), https://doi.org/10.1016/j.jcou.2018.11.006.
[44] V. Dasireddy, B. Likozar, The role of copper oxidation state in Cu/ZnO/Al2O3 catalysts in CO2 hydrogenation and methanol productivity, Renew. Energy 140 (2019) 452–460, https://doi.org/10.1016/j.renene.2019.03.073.
[45] M. Huš, V.D.B.C. Dasireddy, N. Strah Štefančič, B. Likozar, Mechanism, kinetics and thermodynamics of carbon dioxide hydrogenation to methanol on $Cu/ZnAl_2O_4$ spinel-type heterogeneous catalysts, Appl. Catal. B Environ. 207 (2017) 267–278, https://doi.org/10.1016/j.apcatb.2017.01.077.
[46] S.I. Fujita, M. Usui, H. Ito, N. Takezawa, Mechanisms ofmethanol synthesis from carbon dioxide and from carbon monoxide at atmospheric pressure over Cu/ZnO, J. Catal. 157 (1995) 403–413, https://doi.org/10.1006/jcat.1995.1306.
[47] G.J. Millar, C.H. Rochester, S. Bailey, K.C. Waugh, Combined temperature-programmed desorption and fourier-transform infrared spectroscopy study of CO2, CO and H2interactions with model ZnO/SiO2, Cu/SiO2and Cu/ZnO/SiO_2 methanol synthesis catalysts, J. Chem. Soc. Faraday Trans. 89 (1993) 1109–1115, https://doi.org/10.1039/FT9938901109.
[48] A. Bumajdad, A.A. Nazeer, F. Al Sagheer, S. Nahar, M.I. Zaki, Controlled synthesis

of ZrO2 Nanoparticles with tailored size, morphology and crystal phases via Organic/Inorganic hybrid films, Sci. Rep. 8 (2018) 1–9, https://doi.org/10.1038/s41598-018-22088-0.
[49] K.D. Jung, A.T. Bell, Role of hydrogen spillover in methanol synthesis over Cu/ZrO_2, J. Catal. 193 (2000) 207–223, https://doi.org/10.1006/jcat.2000.2881.
[50] K.T. Jung, A.T. Bell, Effects of zirconia phase on the synthesis of methanol over zirconia-supported copper, Catal. Lett. 80 (2002) 63–68, https://doi.org/10.1023/A:1015326726898.
[51] K. Samson, M. Śliwa, R.P. Socha, K. Góra-Marek, D. Mucha, D. Rutkowska-Zbik, J.-F. paul, M. Ruggiero- Mikołajczyk, R. Grabowsk, J. Słoczyński, Influence of ZrO_2 structure and copper electronic state on activity of Cu/ZrO_2 catalysts in methanol synthesis from CO_2, ACS Catal. 4 (2014) 3730, https://doi.org/10.1021/cs500979c.
[52] T. Witoon, J. Chalorngtham, P. umrongbunkitkul, M. Chareonpanich, J. Limtrakul, CO_2 hydrogenation to methanol over Cu/ZrO_2 catalysts: effects of zirconia phases, Chem. Eng. J. 293 (2016) 327, https://doi.org/10.1016/j.cej.2016.02.069.
[53] S. Tada, S. Kayamori, T. Honma, H. Kamei, A. Nariyuki, K. Kon, T. Toyao, K. Shimizu, S. Satokawa, Design of interfacial sites between Cu and amorphous ZrO_2 dedicated to CO2-to-Methanol hydrogenation, ACS Catal. 8 (2018) 7809, https://doi.org/10.1021/acscatal.8b01396.
[54] G. Wang, D. Mao, X. Guo, J. Yu, Enhanced performance of the CuO-ZnO-ZrO_2 catalyst for CO_2 hydrogenation to methanol by WO3 modification, Appl. Surf. Sci. 456 (2018) 403–409, https://doi.org/10.1016/j.apsusc.2018.06.090.
[55] R. Prins, Hydrogen spillover. Facts and fiction, Chem. Rev. 112 (2012) 2714–2738, https://doi.org/10.1021/cr200346z.
[56] J. Im, H. Shin, H. Jang, H. Kim, M. Choi, Maximizing the catalytic function of hydrogen spillover in platinum-encapsulated aluminosilicates with controlled nanostructures, Nat. Commun. 5 (2014) 1–8, https://doi.org/10.1038/ncomms4370.
[57] W. Karim, C. Spreafico, A. Kleibert, J. Gobrecht, J. Vandevondele, Y. Ekinci, J.A. Van Bokhoven, Catalyst support effects on hydrogen spillover, Nature 541 (2017) 68–71, https://doi.org/10.1038/nature20782.
[58] H. Jung, D.R. Yang, O.S. Joo, K.D. Jung, The importance of the aging time to prepare Cu/ZnO/Al_2O_3 catalyst with high surface area in methanol synthesis, Bull. Korean Chem. Soc. 31 (2010) 1241–1246, https://doi.org/10.5012/bkcs.2010.31.5.1241.
[59] J.W. Evans, M.S. Wainwright, A.J. Bridgewater, D. Young, On the determination of copper surface area by reaction with nitrous oxide, Appl. Catal. 7 (1983) 75–83, https://doi.org/10.1016/0166-9834(83)80239-5.
[60] D. Stoilova, V. Koleva, V. Vassileva, Infrared study of some synthetic phases of malachite ($Cu_2(OH)_2CO_3$)-hydrozincite ($Zn_5(OH)_6(CO_3)_2$) series, Spectrochim. Acta - Part A Mol. Biomol. Spectrosc. 58 (2002) 2051–2059, https://doi.org/10.1016/S1386-1425(01)00677-1.
[61] J. Xu, D. Xue, Fabrication of malachite with a hierarchical sphere-like architecture, J. Phys. Chem. B 109 (2005) 17157–17161, https://doi.org/10.1021/jp052864i.
[62] R.L. Frost, W.N. Martens, L. Rintoul, E. Mahmutagic, J.T. Kloprogge, Raman spectroscopic study of azurite and malachite at 298 and 77 K, J. Raman Spectrosc. 33 (2002) 252–259, https://doi.org/10.1002/jrs.848.
[63] G. Moretti, G. Ferraris, G. Fierro, M. Lo Jacono, An XPS study of the reduction process of CuO–ZnO–Al_2O_3 catalysts obtained from hydroxycarbonate precursors, Surf. Interface Anal. 38 (2006) 224–228, https://doi.org/10.1002/sia.2129.
[64] W.R.A.M. Robinson, J.C. Mol, Structure and activity in CO/H2 of Cu/ZnO/Al_2O_3 methanol synthesis catalysts, Appl. Catal. 60 (1990) 61–72, https://doi.org/10.1016/S0166-9834(00)82172-7.
[65] M.M. Günter, T. Ressler, R.E. Jentoft, B. Bems, Redox behavior of copper oxide/zinc oxide catalysts in the steam reforming of methanol studied by in situ X-ray diffraction and absorption spectroscopy, J. Catal. 203 (2001) 133–149, https://doi.org/10.1006/jcat.2001.3322.
[66] T. Lunkenbein, E. Frei, J. Schumann, M. Behrens, M.G. Willinger, R. Schlögl, Local information powers heterogeneous catalysis research: TEM investigation of industrial relevant Cu/ZnO/Al2O3 catalysts for methanol synthesis, Eur. Microsc. Congr, Proc., Wiley-VCH Verlag GmbH & Co, KGaA, 2016, p. 2016, https://doi.org/10.1002/9783527808465.EMC2016.6307.
[67] I.A. Fisher, H.C. Woo, A.T. Bell, Effects of zirconia promotion on the activity of Cu/SiO2 for methanol synthesis from CO/H_2 and CO_2/H_2, Catal. Lett. 44 (1997) 11–17, https://doi.org/10.1023/A:1018916806816.
[68] R. Burch, S.E. Golunski, M.S. Spencer, The role of copper and zinc oxide in methanol synthesis catalysts, J. Chem. Soc. Faraday Trans. 86 (1990) 2683–2691, https://doi.org/10.1039/FT9908602683.
[69] I.A. Fisher, A.T. Bell, A mechanistic study of methanol decomposition over Cu/SiO_2, ZrO_2/SiO_2, and Cu/ZrO_2/SiO_2, J. Catal. 184 (1999) 357–376, https://doi.org/10.1006/jcat.1999.2420.
[70] A.A. Kiss, J.J. Pragt, H.J. Vos, G. Bargemen, M.T. de Groot, Novel efficient process for methanol synthesis by CO_2 hydrogenation, Chem. Eng. J. 284 (2016) 260–269, https://doi.org/10.1016/j.cej.2015.08.101.
[71] F. Arean, G. Italiano, K. Barbera, S. Bordiga, G. Bonura, L. Spadaro, F. Fursteri, Solid-state interactions, adsorption sites and functionality of Cu-ZnO/ZrO_2 catalysts in the CO_2 hydrogenation to CH_3OH, Appl. Catal. A:General 350 (2008) 16–23, https://doi.org/10.1016/j.apcata.2008.07.28.
[72] L. Spadaro, M. Ssantoro, A. Palella, F. Arena, Hydrogen utilization in green fuel synthesis via CO_2 conversion to methanol over new Cu-based catalysts, ChemEngineering 1 (2017) 19, https://doi.org/10.2290/chemengineering1020019.